

# Residual stress analysis and fatigue of multi-pass welded tubular structures

Z. Barsoum

*Royal Institute of Technology, Department of Aeronautical and Vehicle Engineering, Teknikringen 8, 100 44 Stockholm, Sweden*

Received 19 June 2007; accepted 17 November 2007

Available online 5 December 2007

---

## Abstract

The purpose of this study is to investigate the residual stresses near the weld root and the weld toe for multi-pass welded tube-to-plates. Two different tubular joint configurations were studied; a three-pass single-U weld groove for maximum weld penetration and a two-pass fillet (no groove) welded tube-to-plates for minimum weld penetration. A 2D axi-symmetric finite element model was developed to calculate the temperature distribution, HAZ, penetration depth and the residual stress distribution for the sequentially coupled thermo-mechanical analysis. The calculated residual stresses was compared with experimental results and showed qualitatively good agreement. Torsion fatigue tests were performed in order to study crack propagation from the weld root, lower and upper weld toe in mode III. Some of the tube structures were loaded with a static internal pressure in order to separate the root crack and initiate the crack growth in mode III. Another batch was PWHT and fatigue tested, in order to study the influence of residual stresses.

© 2007 Elsevier Ltd. All rights reserved.

*Keywords:* Welding simulation; Residual stresses; Tubular joints; Fatigue; Fracture mechanics

---

## 1. Introduction

Residual stresses have a significant influence on the fatigue strength of welded structures, and it is well known that high tensile residual stresses have a detrimental effect on fatigue life and compressive residual stresses could have a favorable effect on fatigue life. The combination of welding residual stresses with operating stresses to which engineering structures and components are subjected can promote failure by fatigue. The risk of failure can be reduced by various stress relieving processes, such as post weld heat treatment (PWHT). However, the stress distribution for a complex welded structure is usually not known, and conservative assumptions are made of the residual stress distribution when fatigue life predictions are assessed [1,2]. Lack of penetration, lack of fusion or “design root crack” will all act as cracks and if the applied stress intensity variation is high enough and the residual stress level is in tension then fatigue life will be short in comparison if the residual stress is in compression. Investigation regarding the residual stress field on the root side of

---

*E-mail address:* [zuheir@kth.se](mailto:zuheir@kth.se)

welds, and how this field would change during fatigue crack propagation and external loads is important. Consequently, more accurate residual stress distributions are required in the fatigue life assessment, in order to increase the accuracy of the fracture mechanical fatigue life predictions.

In Hansen and Agerskov [3,4] a frame box structure for a two stroke diesel engine was analyzed regarding welding residual stresses, PWHT and fatigue strength. The objective was root crack assessment, and it was found that the as-welded structure had double fatigue life compared to the stress relieved, due to compressive residual stress presence in the root. This compressive stresses gave the higher fatigue resistance compared to the stress relieved specimen.

In Free and Goff [5] a simplified approach was used for residual stress prediction of multi-pass welded tube-to-plate. The residual stress prediction and measurement showed compressive stresses in the weld root and tensile stresses in the weld toe. Finch and Burdekin [2] carried out fracture mechanical calculation for root cracks under residual stresses using the result in [5]. They concluded that compressive residual stress at the weld root tends to close the crack under small tensile load. It always reduces the SIF (stress intensity factor), and hence increase the fracture strength and decrease the crack growth rate in cyclic loading. In Finch [6] evaluation of the interaction between applied stress and residual stress in various geometries of welded joints were studied, and the quantification of welding residual stress effects in the defect assessment of tubular joints were continued.

Michaleris et al. [7] presented a finite element methodology for the incorporation of residual stress effects into fracture assessment. Following the welding simulation, interpolation is used to transfer the computed residual stresses onto fine meshes for evaluation of fracture mechanical parameters.

In this study the residual stresses close the weld root and the weld toe for multi-pass welded tube-to-plates, influence on fatigue resistance and effect of different weld penetrations were investigated.

In this work fatigue testing in torsion has been carried out on tubular joint structures welded with three passes single-U weld groove for maximum penetration, and two-pass fillet weld (no groove) for minimum weld penetration. The objective is to study both weld root and weld toe failure and the effect of residual stresses as welded and post weld heat treated. Another objective was to clarify the significance of the weld penetration depth. Welding simulations in 2D were carried out in order to study the residual stresses, which were verified with residual stress measurements.

## 2. Test objects and welding procedure

The circular tubes and the plates were constructed from structural steel, Swedish type SS142171-91. These are cold drawn post heat treated seamless tubes – STRUCTO 525/ST 52 with yield strength of 576 MPa ( $R_{p0.2}$ ) and ultimate tensile strength of 700 MPa ( $R_m$ ). The plates were hole-drilled circumferentially to fit into the fixture. The welding were carried out in a MAG robot with welding wire Grytgöl GB 74 with a electrode diameter of 1.2 mm and a yield strength of 440 MPa. The welding conditions for the single-U weld groove and the fillet welded tube-to-plates are listed in Tables 1 and 2, respectively. Fig. 1 illustrates the tubular joints and the single-U weld groove.

Table 1  
Welding condition for single-U weld groove welded tube-to-plates

Pass no.	Current (A)	Voltage (V)	Welding speed (mm/s)	Heat input (kJ/mm)
1	210	26	5.1	1.07
2	220	29	4.4	1.45
3	290	30	3.4	2.56

Table 2  
Welding condition for fillet welded (no groove) tube-to-plates

Pass no.	Current (A)	Voltage (V)	Welding speed (mm/s)	Heat input (kJ/mm)
1	280	27	4.7	1.60
2	260	29	3.9	1.93
–	–	–	–	–

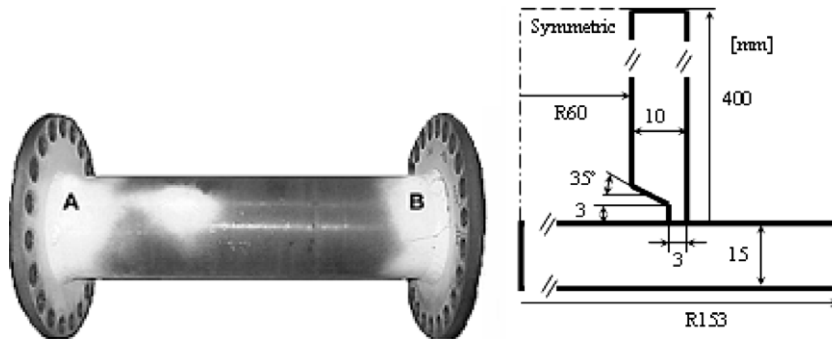


Fig. 1. Welded tubular joint structure an single-U weld groove.

### 3. Finite element model

The thermal and mechanical response of weldments is a 3D problem that requires a large amount of computational time and consequently more time demanding in multi-pass welding. Therefore, it is necessary to develop simplified models and reduce CPU time without decreasing the accuracy. An assumption common in circumferential welding is axi-symmetric, i.e. that the filler weld material is deposited at the same time, hence infinite welding speed. Earlier 2D and 3D welding simulations [8–12] shows that residual stresses in circumferential weldments are quit axi-symmetric, they agrees well with the residual stress measurements and no significant difference between the 2D axi-symmetric and the 3D results were found, except for the residual hoop stress at the surface of the weld. Two axi-symmetric FE-models were built in the FE-software ANSYS 8.1 [13] for the thermal and mechanical analysis; one for the single-U weld groove and one for the fillet welded tube-to-plates, respectively. The same mesh is used in the thermal and the mechanical model and consists of 2983 2D 4-nodes elements (PLANE55 and PLANE42) with 3224 nodes. To this come a number of contact elements (perfect thermal- and mechanical contact) to avoid penetration and closure pressure in the design root crack at the lack of penetration between the tube and the plate. A sequentially coupled analysis was carried out starting with the thermal analysis. The results from the thermal analysis – the temperature distributions, were used as loads in the mechanical model. Fig. 2 illustrates the geometry, dimension and the two

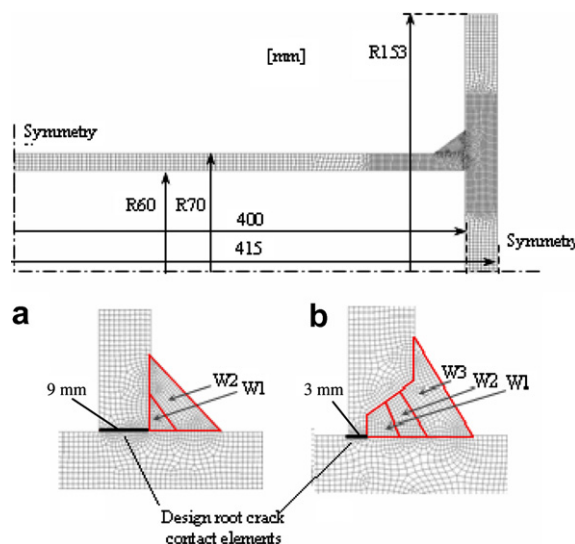


Fig. 2. Axi-symmetric finite elements mesh: (a) two weld passes, no groove; (b) three weld passes single-U weld groove, filler material and design root crack.

different joint configurations considered including the weld filler and the design root crack. The design root crack (lack of penetration) for the single-U weld groove and the no grooved fillet welded tubular structures are 3 and 9 mm, respectively.

**4. Material properties**

The temperature dependent thermal and mechanical material properties for steel SS2172 are shown in Fig. 3. The tube, the plates, HAZ and the filler weld material are assumed to have the same material properties (autogeneous weldments), and these are obtained from Jonsson et al. [14] and Wikander et al. [15] by extracting data points from similar material properties. When the material reaches the solidification temperature the thermal conductivity is assumed to increase 10 times to initiate the fluid flow in the melted zone. The high peaks of the heat capacity are the latent heats due phase transformation (at approx. 700 °C) and heat of fusion (at 1480–1530 °C) corresponding to a latent heat of 260 kJ/kg. Furthermore, cooling by convection during and between the welding passes is modeled by assuming a heat transfer coefficient for all exterior surfaces of 15 (W/°C m<sup>2</sup>). For the mechanical material properties ( $E$ ,  $\nu$ ,  $\sigma_Y$ ,  $\alpha$ ,  $\rho$ ) a cut off temperature,  $T_{\text{cut-off}}$ , was set to 1500 °C, i.e. if the temperature calculated in the thermal analysis is higher than 1500 °C, then the material properties are evaluated at the cut off temperature in the mechanical analysis. The thermal expansion coefficient ( $\alpha$ ) is defined as instantaneously and is set as stress free at 1500 °C for the weld filler material and stress free at 20 °C for the plates and the tube material. The plastic behavior is described by the von Mises criterion

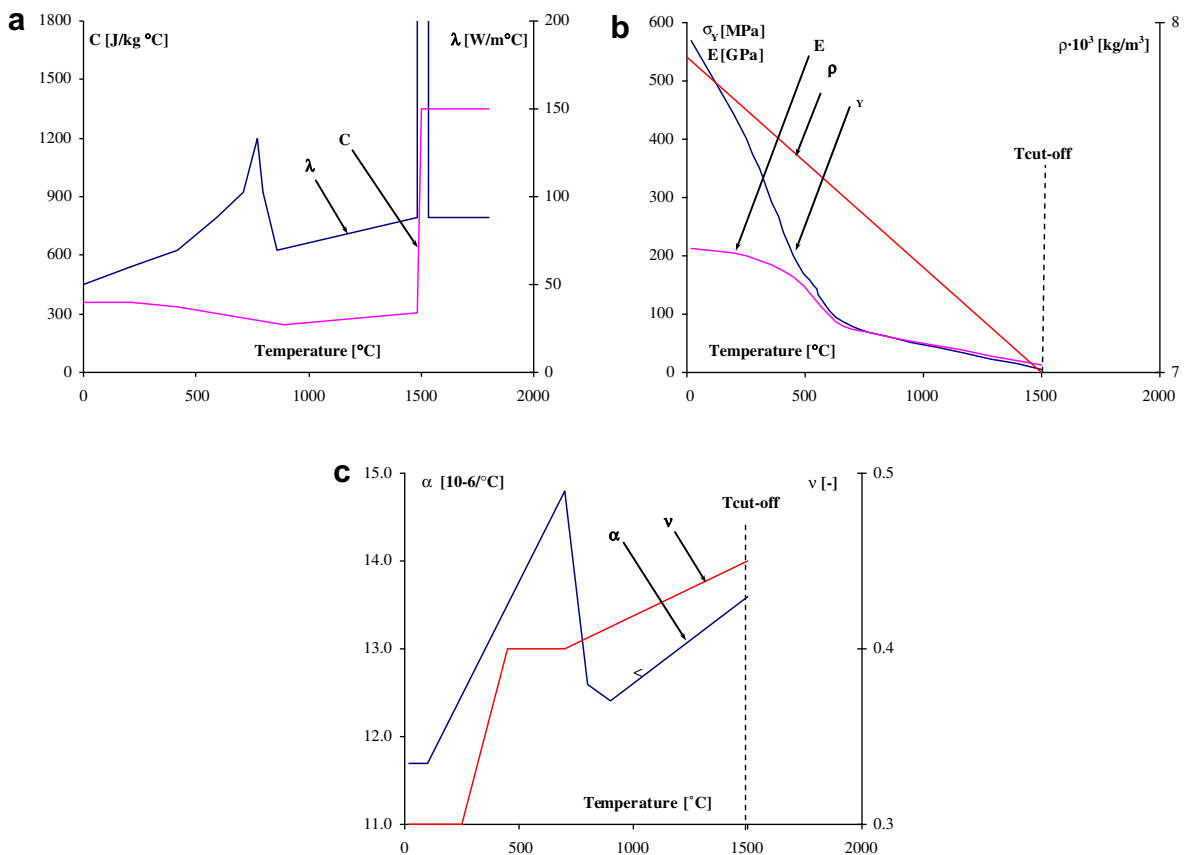


Fig. 3. Thermal and mechanical temperature dependent material properties for SS7142 steel: (a) conductivity ( $\lambda$ ) and heat capacity ( $C$ ) including latent heats of fusion and transformation; (b) density ( $\rho$ ), elastic modulus ( $E$ ) and yield stress ( $\sigma_Y$ ); (c) Poisson's ratio ( $\nu$ ) and thermal expansion coefficient ( $\alpha$ ).

with no hardening. To avoid convergence problems in the numerical calculations the minimum yield limit was set to 10 MPa and the maximum Poisson’s ratio to 0.45.

**5. Thermal analysis**

Sense the geometrical model used in this work is 2D axi-symmetric some assumption is needed for the modeling of the heat source. To simulate arc heating effects during multi-pass welding, the equivalent heat input can be assumed as the combination of both surface and volume heat flux components [16]. To simulate the deposition of weld filler material the technique of element birth and death was utilized (activation and deactivation of elements). The filler material elements were activated at the beginning of the deposition with an initial activation temperature above the melting temperature 1600 °C. Since it is necessary to conserve the energy, the net heat input is reduced because arc efficiency includes the energy added with the filler material. The total net heat input ( $Q_{total}$ ) consists of volume flux ( $Q_{volume}$  (J/sm<sup>3</sup>)), surface flux ( $Q_{surface}$  (J/sm<sup>2</sup>)) and the energy release when the filler material is cooled from activation temperature 1600 °C to room temperature 20 °C. The power balance is given below in Eq. (1):

$$Q_{total} = Q_{deposit} + Q_{volume} + Q_{surface} = \eta UI \tag{1}$$

where  $\eta$  is arc efficiency (~80%),  $U$  is voltage (V) and  $I$  is current (A). The ratio between  $Q_{volume}/Q_{surface}$  can be adjusted to achieve as accurate fusion zone and HAZ as possible compared with the micro-samples, see Fig. 4. In this work the heat input consists of volume heat flux (~30% of  $Q_{total}$ ) and deposition of filler material (~70 % of  $Q_{total}$ ) with activation temperature of 1600 °C. The heat input is active for a certain time,  $t$  (s) depending on the welding speed, ( $v$ ) (m/s) and the diameter, ( $d_f$ ) (m) of the weld filler wire:

$$t = d/v \tag{2}$$

After the heat source is active for  $t$  seconds the weld is cooled down for approximately 10 s between the weld passes, and when the last (second or third) pass is applied the structure is cooled down to room temperature (20 °C). The volume flux,  $q_{volume}$ , is applied according to Eq. (3) assuming constant uniform distribution:

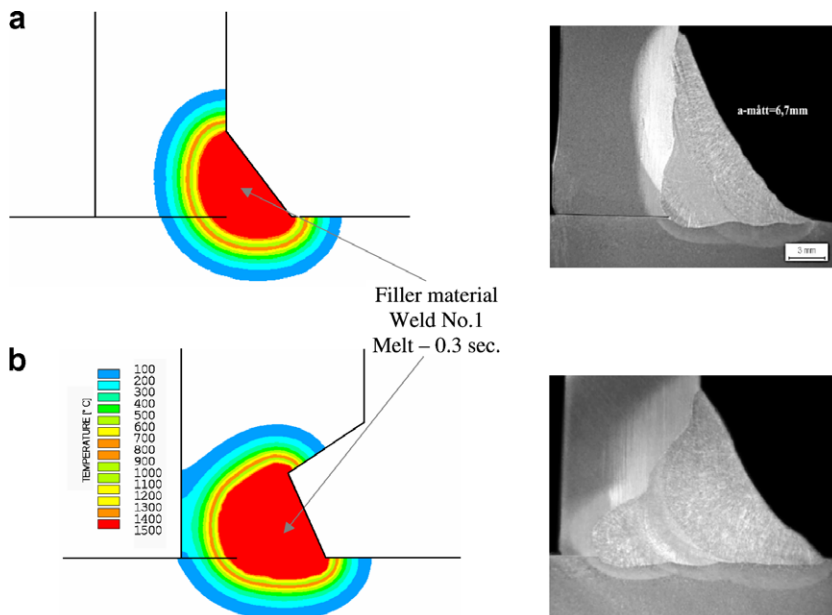


Fig. 4. Temperature fields of the root pass and comparison with micro-samples of the weld penetration profile, fusion zone and HAZ: (a) fillet weld; (b) single-U weld groove.

$$q_{\text{volume}} = \frac{UI\eta \cdot \eta_{\text{volume}}}{A_{\text{FZ}} \cdot d_t} \tag{3}$$

where  $A_{\text{FZ}}$  is the cross-sectional area of the fusion zone,  $\eta_{\text{volume}}$  is the proportion volume flux from total heat flux (30%). This heat source models have been used to approximate simple welding process [17,18]. Micro-samples were produced of the single-U weld groove and the fillet weld. The shape of each layer of filler weld material is predefined in the model based on the experimental micro-samples of the weld penetration profile. The calculated weld penetration profiles, fusion zone and HAZ are shown in Fig. 4 for the first weld.

**6. Residual stresses**

The residual stress in the single-U weld groove welded tube-to-plates is evaluated experimentally by saw cutting and X-ray diffraction technique. The methods are outlined in Radaj [19]. Fig. 5 presents the FEM calculated and experimentally obtained radial and tangential stresses along the top surface of the plate. The measurement point's in the vicinity of the weld line shows a reasonable agreement with the calculated stresses. The FEM calculated stresses was compared with results obtained by Free and Goff [5] for similar welded tubular joints. The trough thickness stress profile at the toe are presented in Fig. 6, the  $y$ -position is normalized by the thickness. Fig. 7 shows the residual stress plot in the axial direction. In the both configuration the “design root crack” is under compression,  $-230$  MPa in the single-U weld groove and  $-120$  MPa in the fillet weld, respectively. Also the weld toe, transition between weld and plate, is under compressive stresses,  $-320$  MPa in the

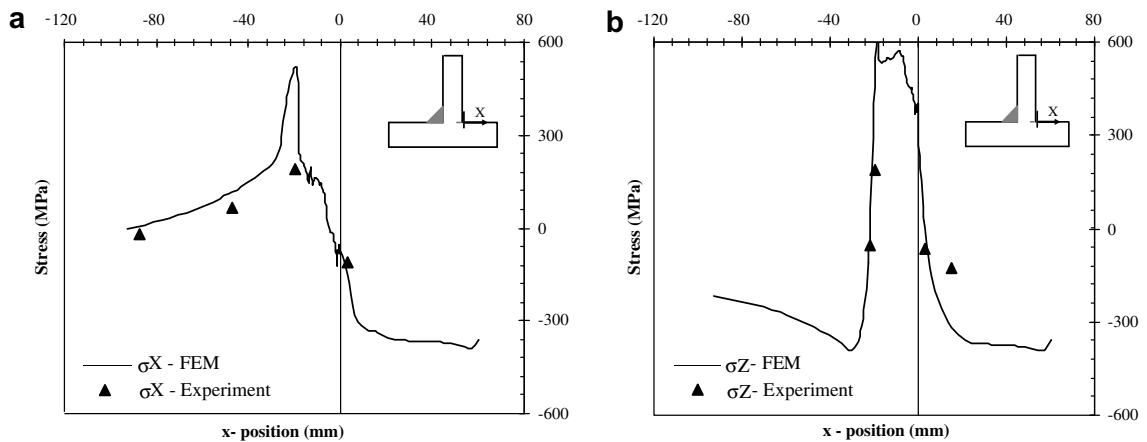


Fig. 5. Predicted and measured residual stress: (a)  $\sigma_x$  – radial transverse stress; (b)  $\sigma_z$  – tangential (hoop) longitudinal stress.

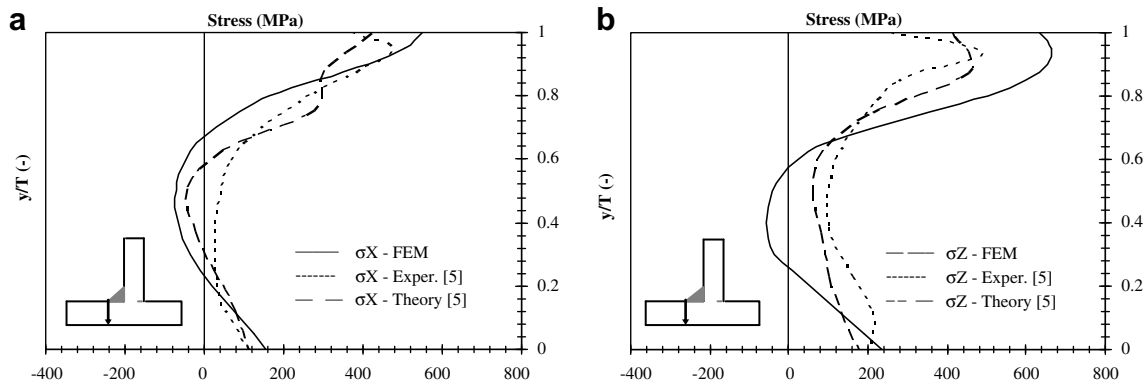


Fig. 6. Trough thickness stress at toe: (a)  $\sigma_x$  – transverse stress; (b)  $\sigma_z$  – longitudinal stress.

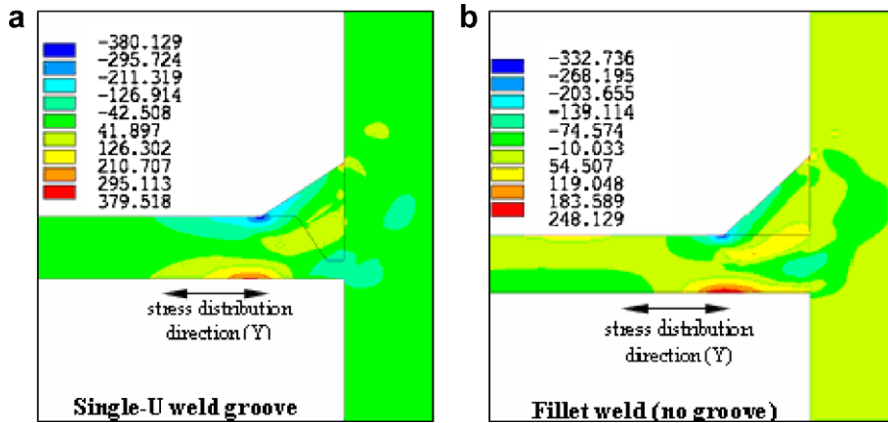


Fig. 7. Contour plots of the residual stress distribution in (MPa) from FEM simulations in the axial direction: (a) single-U weld groove; (b) fillet weld tube to plates.

single-U weld groove and  $-300$  MPa in the fillet weld, respectively. It implies that the compressive residual stress tends to close the root opening and improve the fracture stability at the root and is favorable from a fatigue resistance point of view.

### 7. Fatigue testing

The welded tubular joint structures configurations were produced in series in order to conduct fatigue tests. One objective of the fatigue tests was to quantify the influence of the weld penetration depth on the fatigue resistance. Another important objective was to study the effects of residual stresses and stress relief by post weld heat treatment on the fatigue life and the crack path. The tubular joints were divided in five different batches, see Table 3. The fatigue tests were carried out in a torsion servo-hydraulic test machine with torsion load capacity of  $\pm 25$  kNm. All test were conducted at a stress ratio,  $R$ , of  $-1$  ( $R = \tau_{\min} / \tau_{\max} = \min.$  shear stress/ $\max.$  shear stress). The test were stopped when the root crack ( mostly root failures) have propagate trough the effective throat thickness of the weld – approximately 14 mm for the single-U weld groove types (batch B2 and B3) and approximately 8 mm for the fillet weld type (batch B4). For the other batches (B1 and B5) with only toe failure, the test was stopped when a visible crack on the surface was detected. Sense the compressive residual stresses tends to close the design root crack an internal pressure (hydraulic oil) is applied to separate the crack surfaces and reduces the sliding crack closure influence (friction, abrasion and mutual support between the fracture surfaces), and enable the crack to propagate from the root side. The pressure is static imposed (crack opening mode I) and the fatigue crack propagates in anti-plane shear mode (mode III).

Table 3  
Fatigue test matrix of welded tubular joints

	B1*	B2*	B3*	B4**	B5* (stress relief)
$P_{\text{internal}}$ (MPa)	0	25	15	0	0
FAT <sub>50%</sub> <sup>c</sup>	155	137	132	108	146
FAT according to IIW	142	123	116	83	142
Failure	Toe	Root <sup>a</sup>	Root <sup>a</sup>	Root	Toe <sup>b</sup>

<sup>a</sup> One test object failed at weld toe (between weld and tube) at 18 kNm.

<sup>b</sup> One test object failed at weld toe (between weld and plate) at 20 kNm.

<sup>c</sup> Fatigue strength at two million cycles at a 50% failure probability.

\* Single-U weld groove.

\*\* Fillet weld (no groove).

Fig. 8 shows the fatigue test result (shear stress range vs. cycles to failure) for the different batches. Each point marks fracture of a test specimen. The fatigue resistance data are based on the number of cycles  $N$  to failure, and represented in  $S-N$  curves:

$$N = \frac{C}{\Delta\tau^m} \tag{4}$$

In batch B1 the tubular joints were tested in torsion and no internal static pressure was applied. This batch shows significantly higher fatigue resistance than the other batches. Also the crack path differs from those in B2–B4. The crack initiates from small defects at the weld toe; see Fig. 9a–b, and propagates circumferentially. The residual stress analysis shows tensile stresses in the weld toe region; Fig. 7a–b. Fig. 9c shows the characteristic crack path for specimens in batch B4. The crack is propagating from the root side through the weld. Due to the poor weld penetration depth and the small magnitude of compressive residual stress at the root side no internal pressure was needed to enable the crack to propagate from the root side. For the objects in batch B2, the static internal pressure was 25 MPa and the failure initiation and propagation was from the root side, see Fig. 9d. The internal pressure was lowered to 15 MPa for test objects in batch B3. The majority of the failed tests are from the root, though at lower torsional load ( $\pm 18$  kNm) the failure

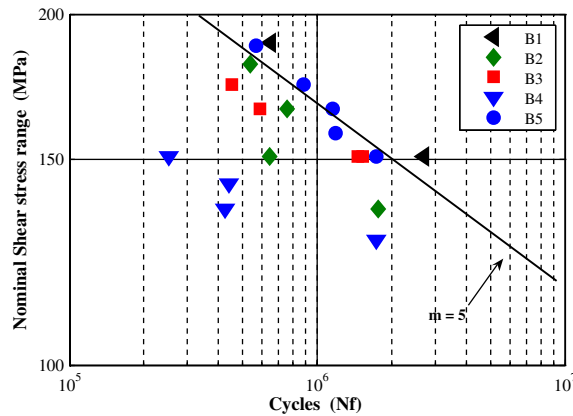


Fig. 8. Results from the fatigue testing in a  $\log(S) - \log(N_f)$  diagram.

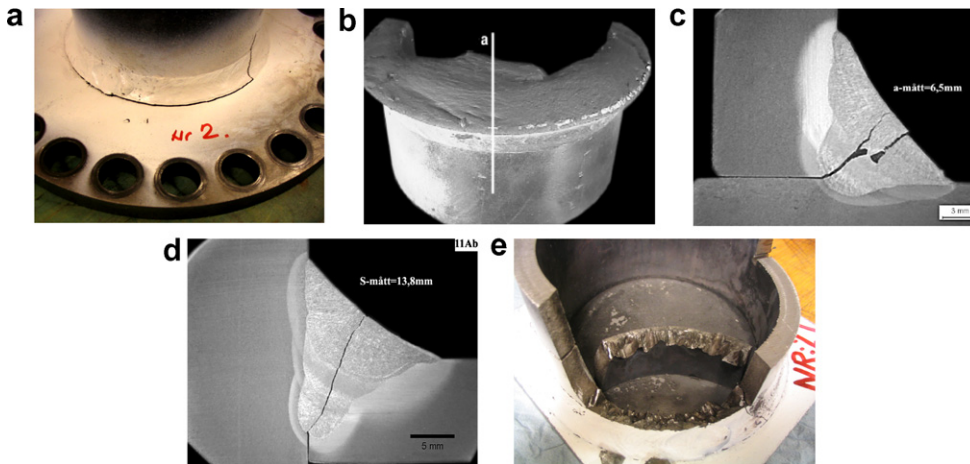


Fig. 9. Different fatigue crack path in the fatigue test of tubular joints: (a) batch B1 – toe (transition between weld-plate) failure; (b) characteristic fracture surface batch B1; (c) batch B4 – root failure; (d) batch B2 and B3 – root failure; (e) batch B5 (stress relieved) – weld toe ( transition between weld-plate) failure.

initiation and propagation is from the toe side. Batch B5 (stress relieved) shows a completely different crack path; “factory roof”, Fig. 9e. The initial defect seems to propagate in mode I, oriented 45° to the tube axis, principal stress, for small torsion loads and for large torsion loads, mode III crack propagation dominates which results in a macroscopically flat mode III fracture surface [20–22].

## 8. LEFM analysis

Pure mode III crack growth rates are typically one or two orders of magnitude smaller than mode I crack growth rate. It is known that cracks do not grow in a mixed mode. They usually grows as mode I cracks, but under certain circumstances they can grow in pure mode II and III. For the case with only torsion load the crack growth rate in mode III is dependent on torque range; higher ranges give higher crack growth rates.

In [20] the influence of static imposed mode I on mode III crack growth was studied. It was concluded that the crack growth rate is not influenced by small axial loads ( $K_I = 0\text{--}3 \text{ MPa}\sqrt{\text{m}}$ ). However if the axial load  $K_I$  is increased to 4–9  $\text{MPa}\sqrt{\text{m}}$  the mode III crack growth rate increases. Also in [23] it was found that only minor variations in the measured crack growth rates if mode I axial load, 0–60  $\text{MPa}\sqrt{\text{m}}$ , were superimposed during mode III crack propagation. Mode III threshold values ( $\Delta K_{IIIth}$ ) are significantly higher than mode I thresholds. According to [22,24] the mode III threshold stress intensity is higher by a factor of 1.35 than for mode I ( $\Delta K_{Ith}/\Delta K_{IIIth} = 0.74$ ). Brown et al. [24] suggest a  $\Delta K_{IIIth} = 12 \text{ MPa}\sqrt{\text{m}}$  and that a transition from mode I to III occurs at 14.4  $\text{MPa}\sqrt{\text{m}}$ . Tschegg [22] suggests that the change from a macroscopically flat (mode III) to a factory roof (mode I) type determines the threshold value for mode III crack propagation, because mode III crack growth could not be obtained at  $\Delta K_{III}$  values below this threshold.

Fig. 10 shows crack growth rates for mode I and III. The mode I growth is dominated when the stress intensity is low and mode III growth dominates the high stress intensity region. It indicates that mode III could be neglected under mixed mode conditions in the initial phase of crack propagation [25].

Fig. 11 shows the FEM calculated stress intensity factors ( $\Delta K_{III}$ ) for the different crack paths observed in the fatigue test in Fig. 9. Assuming a 0.1 mm initial crack at the weld toes and the lack of penetration from the root side as a initial crack (3 mm for the single-U weld groove and 9 mm for the fillet weld) it reveals due to the low SIF the tubes failed from the lower toe will have a slightly higher fatigue life compared with those failed from other crack sites. For the root failures the fatigue capacity is determined by the effective weld throat, 14 and 8 mm, and the size of the design root crack, 3 and 9 mm, for the single-U and the fillet welded tubes, respectively.

A linear elastic fracture mechanical analysis was also conducted by including the predicted residual stresses in the FE model in order to investigate the influence of the lack of penetration from the root side, internal pressure and the residual stress for the single-U weld groove welded tubular structure. The predicted residual stresses were mapped to the linear elastic FE model with the lack of penetration as a preexisting crack (3 mm),

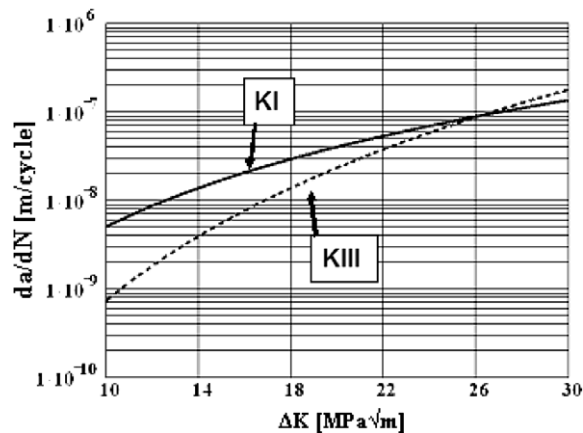


Fig. 10. Crack growth rates for mode I and III.

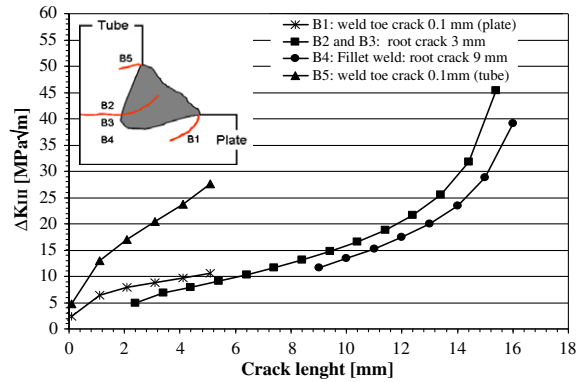


Fig. 11. Stress intensity factor range in mode III ( $\Delta K_{III}$ ),  $\Delta\tau_{nom} = 166$  MPa, for the different crack paths observed from the fatigue tests.

Table 4

Result from LEFM analysis including residual stresses and internal pressure for single-U weld groove tubular structure

$a_i$ (mm)	Pressure (MPa)	$K_I$ (MPa√m) <sub>pressure</sub>	$K_I$ (MPa√m) <sub>residual</sub>	$K_I$ (MPa√m) <sub>total</sub>
3 <sup>a</sup>	0	0	−9.52	−9.52
3 <sup>a</sup>	15	10.07	−9.52	0.55
3 <sup>a</sup>	25	16.7	−9.52	7.18
9 <sup>a</sup>	0	0	−8.23	−8.23
0.1 <sup>b</sup>	0	0	9.32	9.32
0.1 <sup>c</sup>	0	0	−8.75	−8.75

<sup>a</sup> Lack of penetration; root crack. B2, B3 and B4.

<sup>b</sup> Weld toe crack (weld-plate). B1.

<sup>c</sup> Weld toe crack (weld-tube). B5.

the internal pressure was applied and the opening mode stress intensity factor,  $K_I$ , were calculated for both the residual stresses and the internal pressure. The FE crack growth simulation program Franc2D [26] was employed for this reason. Table 4 summarizes the LEFM analysis considering the internal pressure and the simulated residual stresses. The total static  $K_I$  is the sum of  $K_I$  due to the internal pressure and  $K_I$  due to the residual stress. When no internal pressure is applied  $K_I$  is compressive and keeps the crack closed. When the internal pressure is increased to 15–25 MPa ( $K_I = 0.55$ – $7.18$  MPa√m) for the tubular structure with the 3 mm root crack the crack will be open and mode III crack propagation is enabled from the weld root side although  $\Delta K_{III}$  is small compared with the 9 mm root crack for the fillet welded tubular structure, see Figs. 9 and 11. The  $K_I$  values due to residual stress are also calculated for the assumed 0.1 mm toe cracks; at the plate and at the tube, respectively. The 0.1 mm toe crack (plate) is tensile due to the tensile residual stress at the weld toe, 9.32 MPa√m, and will keep the crack open during the cyclic loading. The 0.1 mm toe crack (tube) is compressive due to the compressive residual stress at the weld toe, −8.75 MPa√m, and will keep the crack closed during the cyclic loading until the compressive residual stresses are eliminated, e.g. when stress relieving by post weld heat treatment as in batch B5.

## 9. Conclusion

Residual stress prediction and measurement was carried out on welded tubular joint structures containing a lack of penetration, with single-U weld groove and no groove, respectively. Two-dimensional finite element welding simulation was carried out on the multi-pass welded tubular joint structures. The calculated temperatures and residual stresses were compared with measurements. Fatigue tests were also performed. The objective was to study weld toe and root cracking and the influence of residual stresses. The following conclusions were made:

1. Good agreement is achieved between micro-samples and FE analysis of the weld penetration profile and the fusion zone by using a simplified heat input and a 2D axi-symmetric model. The calculated residual stresses are in qualitative good agreement with the experimental obtained.
2. The design root crack is under favorable compressive residual stresses in the welded tube-to-plates configurations (with groove and no groove). This keeps the root crack closed and higher the fracture stability.
3. The lack of penetration size (root error) has a major influence on the fatigue strength assessed from the root side in combination with compressive residual stresses.
4. The fatigue test result shows no increase in fatigue strength for the stress relieved tubular structures compared with the as-welded, due to the relieving of the compressive residual stresses.
5. Depending on the level of the torque range ( $\Delta K_{III}$ ), the static imposed  $K_I$  and the stress relieving different crack paths were received in the fatigue tests. At low axial loads  $K_I$  (10 MPa $\sqrt{m}$ ) and low torsion load ( $\Delta\tau = 136\text{--}150$  MPa) the failure mode shifts from root to toe failure.
6. Mode III crack growth is sensitive to the magnitude of the static mode I loading.

### Acknowledgements

The authors would like to thank Mr. Nenad Mrden at Volvo Construction Equipment AB for carrying out the fatigue tests. Also Mr. Gunnar Åkerström and Mr. Mirsattar Hejasiffar at Volvo Metals Laboratory are acknowledged for assistance with the residual stress measurements. Professor Jack Samuelsson at KTH and Professor Lars Erik Lindgren are acknowledged for valuable discussions.

### References

- [1] Martinsson J. Comparisons between different contemporary FCG programs on welded components. IIW Document. No. XIII-1994-03. 2003.
- [2] Finch D, Burdekin FM. Effect of welding residual stresses on significance of defects in various types of welded joint. *Eng Fract Mech* 1992;41(5):721–35.
- [3] Hansen JL. Residual stresses from welding of large diesel engine structures. In: Samuelsson J, editor. *Proceedings of design and analysis of welded high strength steel structures*. EMAS; 2002. p. 345–72.
- [4] Hansen AV, Ågerskov H. Fatigue assessment of root defects in the welded structures of a diesel engine. In: Samuelsson J, editor. *Proceedings of design and analysis of welded high strength steel structures*. EMAS; 2002. p. 373–89.
- [5] Free JA, Porter Goff RF. Predicting residual stress in multi-pass weldments with the finite element method. *Comput Struct* 1989;32(2):365–78.
- [6] Finch D. Effect of welding residual stresses on significance of defects in various types of welded joint-II. *Eng Fract Mech* 1992;42(3):479–500.
- [7] Michaleris P, Kirk M, Mohr W, McGaughy T. Incorporation of residual stress effects into fracture assessment via the finite element method. *Fatigue and fracture mechanics*. In: Underwood JH, Macdonald BD, Mitchell MR, editors. *American society for testing and materials*, vol. 28. ASTM STP 1321; 1997.
- [8] Karlsson CT. Finite element analysis of temperature and stresses in a single-pass butt-welded pipe – influence of mesh density and material modeling. *Eng Comput* 1989;6:133–41.
- [9] Lindgren L-E, Karlsson L. Deformations and stresses in welding of shell structures. *Int J Numer Meth Eng* 1988;25:635–55.
- [10] Karlsson RI, Josefson BL. Three-dimensional finite element analysis of temperatures and stresses in a single-pass butt-welded pipe. *ASME J Press Vessel Tech* 1990;112:76–84.
- [11] Murthy YVLN, Rao Venkata G, Iyer Krishna P. Numerical simulation of welding and quenching process using transient thermal and thermo-elasto-plastic formulations. *Comput Struct* 1996;60(1):131–54.
- [12] Josefson BL, Karlsson CT. FE-calculated stresses in a multi-pass butt-welded pipe – a simplified approach. *Int J Vessel Piping* 1989;38:227–43.
- [13] ANSYS guide. ANSYS release 8.1 Swanson Analysis Systems: Houston.
- [14] Jonsson M, Karlsson L, Lindgren LE. Deformations and stresses in butt-welding of large plates with special reference to the mechanical material properties. *J Eng Math Tech* 1985;107:265–70.
- [15] Wikander L, Karlsson L, Näsström M, Webster P. Finite element simulation and measurement of welding residual stresses. *Model Simul Mater Sci Eng* 1994;2:845–64.
- [16] Goldak J, Bibby M, Moore J, House R, Patel B. Computer modeling of heat flow in welds. *Metall Trans B* 1986;17B:587–600.
- [17] Bang IW, Son YP, OH KH, Kim YP, Kim WS. Numerical simulation of sleeve repair welding of in-service gas pipelines. *Weld J* 2002;273–82.
- [18] Sabapathy PN, Wahab M, Painter MJ. Numerical models of in-service welding of gas pipelines. In: *International conference on advances in materials and processing technologies*. 1999. p. 663–74.

- [19] Radaj D. Welding residual stresses and distortion – calculation and measurement. DVS Verlag; 2003. ISBN 3-87155-791-9.
- [20] Tschegg EK. The influence of static I load Mode and  $R$  ratio on Mode III fatigue growth behavior in mild steel. *J Mater Sci Eng* 1983;59:127–37.
- [21] Vaziri A, Nayeb-Hashemi H. The effect of crack surface interaction on the stress intensity factor in Mode III crack growth in round shafts. *Eng Fract Mech* 2005;72:617–29.
- [22] Tschegg EK. A contribution to Mode III fatigue crack propagation. *Mater Sci Eng* 1982;54:127–36.
- [23] Tschegg EK, Ritchie RO, McClintock FA. On the influence of rubbing fracture surfaces on fatigue crack propagation in Mode III. *Int J Fatigue* 1983(January):29–35.
- [24] Brown MW, Hay E, Miller KJ. Fatigue at notches subjected to reversed torsion and static axial loads. *Fatigue Fract Eng Mater Struct* 1985;8(3):243–58.
- [25] Byggnevi M. Crack growth parameters useful in fatigue analysis of welded joints in steel: a literature survey. Report TRITA-AVE 2005-20. Lic thesis. Stockholm: Department of Aeronautical and Vehicle Engineering, Royal Institute of Technology; 2005. Paper C.
- [26] FRANC2D. Version 3.2 <<http://www.cfg.cornell.edu/>>.